This document is the accepted manuscript version of a published work that appeared in final form in Nature Chemistry, 2018, 10, 24-30, DOI: 10.1038/NCHEM.2874

Polyoxometalate electrocatalysts based on earth-abundant metals for efficient water oxidation in acidic media

Marta Blasco-Ahicart, Joaquín Soriano-López, Jorge J. Carbó, Josep M. Poblet and J. R. Galan-Mascaros

Water splitting is a promising approach to the efficient and cost-effective production of renewable fuels, but water oxidation remains a bottleneck in its technological development because it largely relies on noble-metal catalysts. Although inexpensive transition-metal oxides are competitive water oxidation catalysts in alkaline media, they cannot compete with noble metals in acidic media, in which hydrogen production is easier and faster. Here, we report a water oxidation catalyst based on earth-abundant metals that performs well in acidic conditions. Specifically, we report the enhanced catalytic activity of insoluble salts of polyoxometalates with caesium or barium counter-cations for oxygen evolution. In particular, the barium salt of a cobalt-phosphotungstate polyanion outperforms the state-of-the-art IrO_2 catalyst even at pH < 1, with an overpotential of 189 mV at 1 mA cm^{-2}. In addition, we find that a carbon-paste conducting support with a hydrocarbon binder can improve the stability of metal-oxide catalysts in acidic media by providing a hydrophobic environment.

Water is vastly preferred as a source for hydrogen—one of the most promising green fuels for the establishment of a sustainable and environmentally friendly energy cycle[1]. This closed cycle would work using renewable energy to split water into oxygen and hydrogen, and recombining them back into water via fuel cells, for example, to extract the stored energy. However, water-splitting technologies are still far from being economically competitive for solar fuel production. This is a major issue to be overcome in order to support a societal change in the energy paradigm, in particular when very cheap hydrogen is currently available from steam reforming[2]. Therefore, tremendous research effort is being made in the field to find viable solutions to reduce solar fuel production costs, with most being focused on electrochemical processes. Finding cost-effective, earth-abundant, efficient and robust catalysts for water splitting is essential.

Recently, low-cost catalysts for the hydrogen evolution reaction (HER) have been described for multiple working conditions and a large pH range[3–5]. However, the oxygen evolution reaction (OER) remains a more difficult problem, especially in acidic media[6]. Water oxidation is a complex four-electron redox process that produces protons and oxygen, and typically requires very high overpotentials η. Earth-abundant and inexpensive water oxidation catalysts (WOCs) that match all these requirements have been found for alkaline or neutral media applications. However, only noble-metal oxides such as RuO_2 or IrO_2 fulfil the technological requirements in acidic conditions[7], and RuO_2 suffers from rapid deactivation[8].

Acidic solutions appear to be preferred as media to carry out water electrolysis. Hydrogen production is much easier at lower pH, where the proton (as reagent) concentration is higher[9,10]. Alkaline electrolysis has additional drawbacks, such as more difficult product separation or carbonation. The lack of a low-cost alternative WOC to IrO_2 in acidic media remains a major challenge in the field.

Transition-metal oxides have been studied for several decades as WOCs, with excellent results[11–18]. Unfortunately, all lose their remarkable activity on lowering the pH[19,20]. Only cobalt oxides appear to retain interesting activity at neutral pH, with the help of ancillary electrolytes[21,22]. At higher proton concentrations, catalytic performance is insufficient and corrosion becomes a major issue. Under these acidic conditions, manganese oxides, for example, support only very low current densities, and doping or electrochemical treatments are being studied to improve their stability and performance[23,24]. Nanostructured cobalt oxides can sustain good current densities, but for short periods of time due to corrosion[25]. However, the latter may be incorporated into the hydrogen production scheme to improve overall yields[26]. Unfortunately, neither of these clever strategies can compete with the performance of IrO_2.

As an alternative to oxides, cobalt-containing polyoxometalates (Co-POMs) have shown to be promising homogeneous earth-abundant WOCs in close-to-neutral pH[27–30]. Although their activity has been subject to close scrutiny[31–33], there is no doubt that they are genuine molecular WOCs under controlled working conditions[34–37]. Interestingly, we have demonstrated that Co-POMs maintain their catalytic activity in heterogeneous conditions when supported on modified electrodes as insoluble caesium salts[38].

Here, we disclose the excellent catalytic activity of water-insoluble Co-POM salts in acidic media. Modified electrodes incorporating barium salts of Co-POMs promote OER during water electrolysis experiments, with superior performance to the state-of-the-art IrO_2 in sulfuric acid solution (1 M). Lower onset potentials, higher current densities at lower overpotentials and Faradaic oxygen evolution demonstrate that barium Co-POM salts are a real alternative to the corresponding noble-metal champions. This is the first time that a competitive activity has been found in a low-cost, earth-abundant material, opening unprecedented

[1]Institute of Chemical Research of Catalonia (ICIQ), The Barcelona Institute of Science and Technology (BIST), Av. Països Catalans 16, E-43007 Tarragona, Spain. [2]Departament de Química Física i Inorgànica, Universitat Rovira i Virgili, Marcel.lí Domingo 1, E-43007 Tarragona, Spain. [3]ICREA, Passeig Lluis Companys, 23, E-08010 Barcelona, Spain. †These authors contributed equally to this work. *e-mail: jrgalan@iciq.es

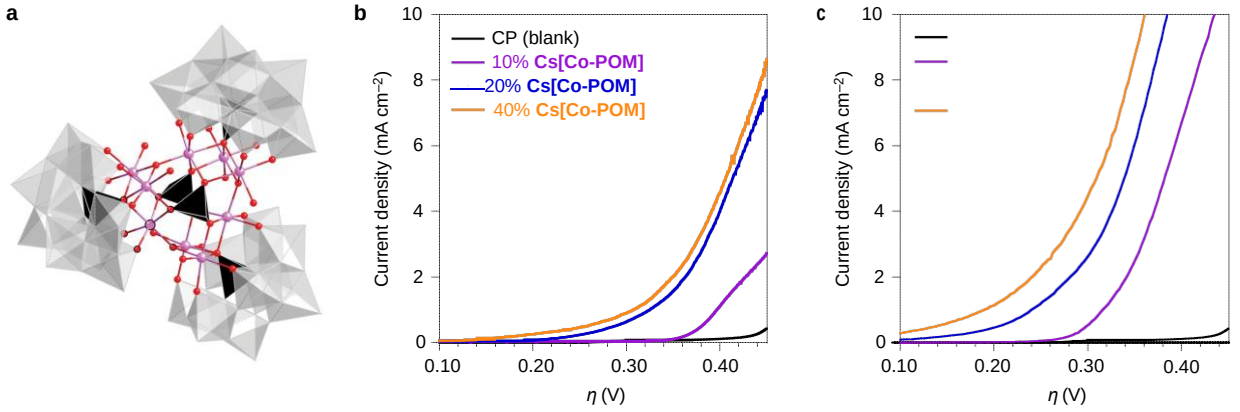

Figure 1 | Electrochemical behaviour of Co-POM/CP electrodes. a, Molecular structure of the $[Co_9(H_2O)_6(OH)_3(HPO_4)_2(PW_9O_{34})_3]^{16-}$ cluster. Co, pink; O, red; WO_6, grey octahedra; PO_4, black tetrahedra. b, Linear sweep voltammetry in H_2SO_4 (1 M) solution with a Cs[Co-POM]/CP blend working electrode for different catalyst contents. The increment in current indicates the onset of electrocatalytic water oxidation. CP: blank experiment with a carbon-paste-only electrode. c, Same experiments with a Ba[Co-POM]/CP blend electrode, showing the lower overpotentials needed to reach even higher currents. This indicates a better electrocatalytic energy efficiency overall, because current is proportional to oxygen evolution.

opportunities to develop technologically and economically viable acid water electrolysis.

Results and discussion

Electrochemistry. Due to the high level of interest in acid water oxidation catalysis, we decided to test the activity, in acidic media, of the caesium salt of the $[Co_9(H_2O)_6(OH)_3(HPO_4)_2(PW_9O_{34})_3]^{16-}$ cluster (Co_9, Fig. 1a), which was obtained by simple metathesis of the corresponding potassium salt as $Cs_{15}K[Co_9(H_2O)_6(OH)_3(HPO_4)_2(PW_9O_{34})_3]\cdot 28H_2O$ (Cs[Co-POM]). We blended this salt with commercial carbon paste (CP, formed from carbon black and an organic oil binder) to obtain a modified electrode to be used as the anode in water electrolysis experiments in H_2SO_4 solution (1 M), without any additional electrolyte. The three-electrode configuration was completed with a Pt mesh as counter-electrode and a Ag/AgCl reference electrode. We investigated the electrochemical activity of Cs[Co-POM]/CP blends using linear sweep voltammetry (LSV). The current densities showed a rapid increase deviating from the flat response of the CP, indicating the appearance of catalytic currents (Fig. 1b). We optimized the catalyst content following the LSV response. Catalytic performance shows optimum activity for blends at 30–40% content (in weight) with a minimum onset potential of 1.42 V vs NHE ($\eta = 196$ mV). Blends with more than 50% content became too brittle for accurate measurements, so we limited the maximum catalyst content to 40% for all further studies.

We carried out analogous electrochemical studies substituting Cs^+ with Ba^{2+}. This heavy alkaline earth dication forms the water-insoluble salt $Ba_8[Co_9(H_2O)_6(OH)_3(HPO_4)_2(PW_9O_{34})_3]\cdot 55H_2O$ (Ba[Co-POM]). To our surprise, Ba[Co-POM]/CP electrodes showed a significantly better electrocatalytic performance. The LSV data show onset potentials as low as $\eta = 88$ mV and higher current densities in the potential range studied (Fig. 1c and Supplementary Fig. 1). This huge improvement in voltage efficiency suggests a strong influence of the counter-cation in electrocatalysis kinetics, because both salts contain the same active Co-POM. The origin of this positive effect could be related to better electron transfer kinetics. However, without further experimental evidence, we cannot discount that it is related to higher hydration, a different surface area/interface or lower crystallinity.

Comparative electrochemistry. It is difficult to compare OER catalytic activities[39], because many parameters affect the overall performance, including particle size, active surface area, accessibility to active sites, electrode geometry, electronic interface and so on. To put our Co-POM results into context, we carried out the same experiments using an IrO_2/CP blend to mimic identical working conditions. As shown in Fig. 2a, no IrO_2/CP blend can match the catalytic activity of the Co-POM electrodes at low overpotentials with the same catalyst content by weight. The Ba[Co-POM]/CP blend exceeds the performance of the noble-metal oxide in the entire potential range studied. Lower potentials are needed to reach the same current densities (Table 1), including a remarkable 246 mV difference for the onset potential of water oxidation and 97 mV to reach a current density of 10 mA cm^{-2}. The superior performance of Ba[Co-POM]/CP is even more evident if we take into account the total number of possible active sites (Supplementary section 'Active sites calculation') in each modified electrode, given the different molecular weight. For instance, with the same catalyst weight, IrO_2/CP blends contain at least five times more active sites than the corresponding Ba[Co-POM]/CP blend. Thus, Ba[Co-POM] easily outperforms the kinetics of the best state-of-the-art OER catalyst in acidic media, per weight and per mol, while being obtained from inexpensive starting materials (barium, cobalt, phosphate and tungstate), representing the first competitive catalyst of its kind. Such lower overpotentials would improve the voltage efficiency of a water-splitting device by a large margin, maximizing energy efficiency.

We also studied the Tafel plots for these catalysts (Fig. 2b), with steady-state current density values in the $0.0 < \eta < 0.4$ range. The Tafel slopes were 66 mV dec^{-1} (IrO_2/CP), 98 mV dec^{-1} (Cs[Co-POM]/CP) and 97 mV dec^{-1} (Ba[Co-POM]/CP). The Tafel slope depends exclusively on the rate-determining step of an electrochemical process. The IrO_2/CP slope is typical of this catalyst[40], indicating chemically controlled kinetics. The Co-POM slopes are higher, indicating competition between a chemical and an electron-transfer limiting step. This is not surprising given the insulating nature of the Co-POM salts when compared with the high conductivity of IrO_2. Even with a higher Tafel slope, the Ba[Co-POM]/CP blends reach higher currents in a large potential range because of their lower onset potentials. This allows an overall lower energy consumption to be sustained and thus a higher energy efficiency. Extrapolating the Tafel plots (only valid if the rate-determining step of the mechanism does not change with potential), IrO_2 would match the performance of Ba[Co-POM] at overpotentials greater than 0.7 V. The identical slope for both Co-POMs suggests the same oxygen evolution mechanism is taking place in both cases, as expected, because both Co-POMs contain the same active sites.

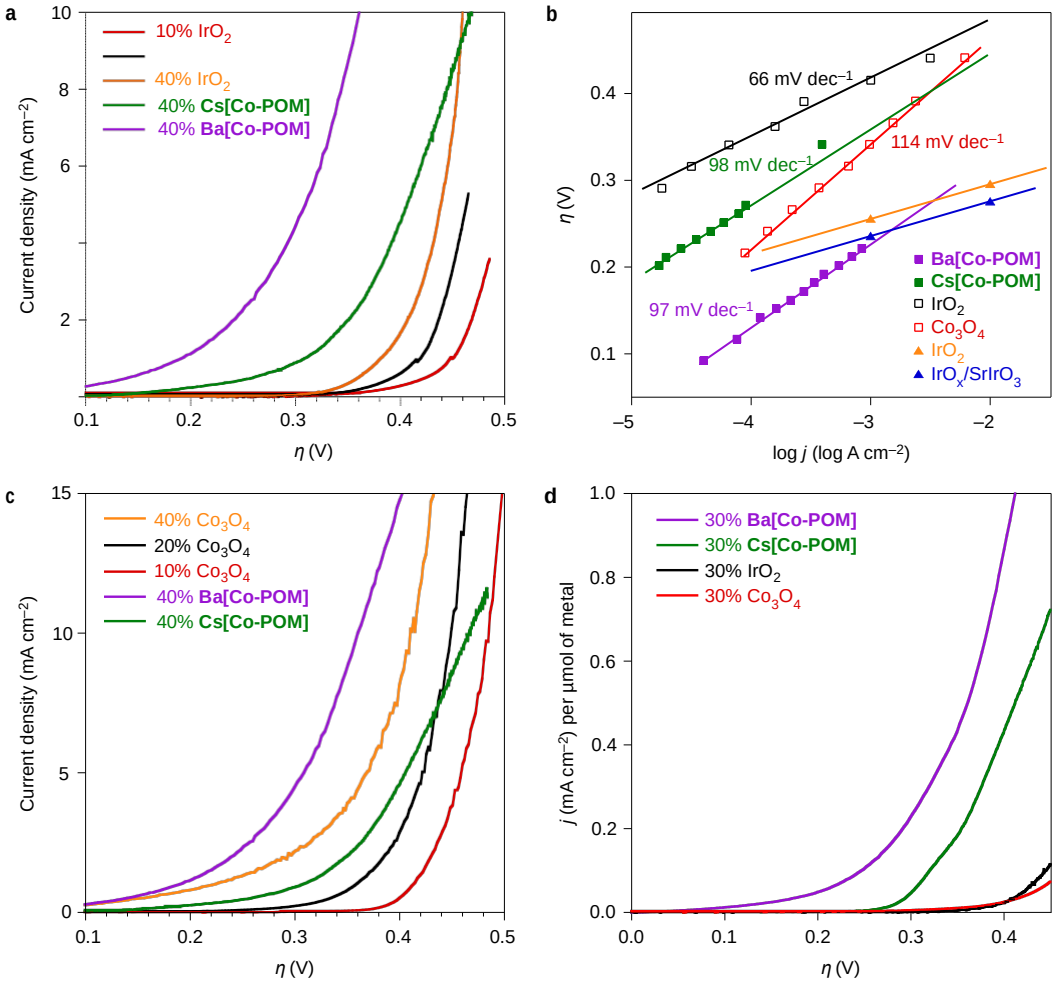

Figure 2 | Comparative electrochemical behaviour of catalyst/CP electrodes in acidic media, highlighting the superior activity of Co-POM modified electrodes for oxygen evolution. Ba[Co-POM]/CP reaches higher currents at lower overpotentials in the entire range studied. When compared with state-of-the-art nanostructured IrO_2-based catalysts, Ba[Co-POM]/CP remains a competitive non-noble alternative, in particular at low overpotentials. a, Linear sweep voltammetry in H_2SO_4 (1 M) solution with an IrO_2/CP blend working electrode for different catalyst content, compared with Cs[Co-POM]/CP and Ba[Co-POM]/CP electrodes. b, Tafel region for 30% catalyst/CP blends from steady-state chronopotentiometry experiments in H_2SO_4 (1 M) solution. Orange and blue triangles are taken from the literature, and represent the state of the art for IrO_2 and IrO_x/$SrIrO_3$, respectively[41,42]. c, Linear sweep voltammetry in H_2SO_4 (1 M) solution with a Co_3O_4/CP blend working electrode for different catalyst content, compared with Cs[Co-POM]/CP and Ba[Co-POM]/CP electrodes. d, Normalized linear sweep voltammetry in H_2SO_4 (1 M) solution for 30% catalyst/CP blends with respect to the total active metal content (Co or Ir), showcasing the superior Ba[Co-POM] activity per mol.

We need to mention that the IrO_2 activity we found in our CP blends is not comparable with state-of-the-art IrO_2 preparations[41]. Additionally, Jaramillo et al. reported how nanostructuring of IrO_x/$SrIrO_3$ blends enhances their already high catalytic activity[42]. Nevertheless, our Ba[Co-POM]/CP electrodes exhibit better catalytic activity at low overpotentials than the best IrO_2 results available[41,42] and are still competitive at moderate current densities up to 10 mA cm^{-2} (Fig. 2b).

An important issue with Co-POMs is the possibility to evolve into the corresponding CoO_x species (a competitive WOC) during water oxidation. Indeed, CoO_x has been identified as the major active phase in water oxidation catalysis when starting with Co-POMs under certain experimental conditions[31,32]. We carried out the same experiments starting with Co_3O_4 to gather additional evidence on the possible participation of traces of adventitious CoO_x. We observed that the water oxidation activity of Co_3O_4/CP electrodes is clearly better than what has been typically reported for this WOC in acid[26]. This suggests that the use of a hydrophobic binder and an appropriate conducting support could extend the use of classic metal oxides into acidic media.

Although Co^{2+} is a competent WOC[20], we can rule out the participation of any homogeneous species during these experiments, because post-electrocatalytic elemental analysis data (from inductively coupled plasma optical emission spectrometry, ICP-OES) confirmed the absence of any metal in solution (Supplementary Table 1).

The LSV data for the Co_3O_4/CP blends (Fig. 2c and Table 1) show an electrocatalytic performance close to that of Cs[Co-POM]/CP by weight, reaching a very low onset potential for high catalyst contents. The Tafel plots indicate a different rate-determining step, with significantly higher slopes over 110 mV dec^{-1} (Fig. 2b). These oxide blends thus cannot match the Ba[Co-POM]/CP modified electrodes when reaching significant current densities (over 1 mA cm^{-2}). As described already, it is worth mentioning that these comparisons by weight are unfair to the Co-POM catalysts. At the same weight, the number of active sites in an oxide electrode is about one order of magnitude higher due to its lower molecular weight and higher density of active sites. If we normalize the current density data taking into account the total number of Co centres, the activity of both Co-POM/CPs is remarkably better (Fig. 2d).

Table 1 | Comparison of linear sweep voltammetry data for Co-POM/CP electrodes with the corresponding iridium and cobalt oxide blends as a function of catalyst content.

cat/CP (%)	Cs[Co-POM]	Ba[Co-POM]	IrO_2	Co_3O_4
		η_{onset} (mV)		
40	196	88	334	90
30	236	103	335	196
20	246	164	363	305
10	363	280	393	386
		η (mV) @ j = 1 mA cm^{-2}		
40	306	189	379	221
30	316	244	388	311
20	324	240	416	357
10	395	314	447	412
		η (mV) @ j = 10 mA cm^{-2}		
40	466	361	458	410
30	>500	384	480	446
20	>500	404	>500	454
10	>500	434	>500	485
		pH		
40	0.1	0.2	0.1	0.2
30	0.2	0.1	0.2	0.2
20	0.3	0.2	0.1	0.2
10	0.2	0.2	0.1	0.2
		cat (total mg)		
40	13	11	14	19
30	11	9	12	14
20	8	7	9	8
10	4	4	5	4

The exact pH of each 1 M H_2SO_4 solution was confirmed by direct measurements. Cat, catalyst.

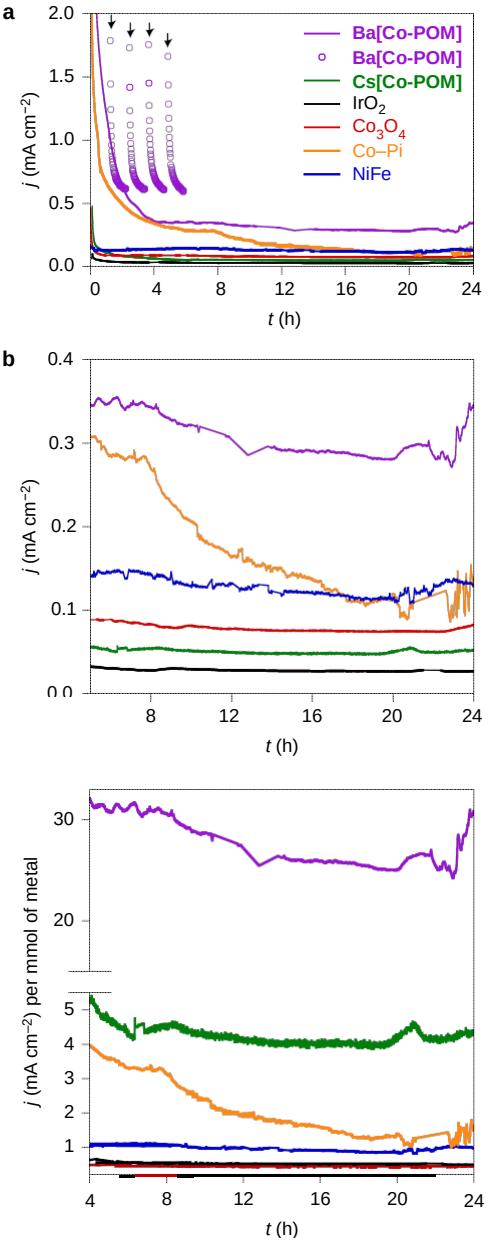

Figure 3 | Stability and benchmarking of catalyst/CP electrodes. Chronoamperometry data in H_2SO_4 (1 M) solution at a constant anodic overpotential of 250 mV with 30% catalyst/CP blends. a, Over a period of 24 h, the Ba[Co-POM] exhibits superior currents and a robust response after 4 h. The initial fast decay during the first hours is associated with a capacitance event and is not due to catalyst fatigue. This was confirmed by an intermittent analogous process (empty circles), where this trend is reproduced. Arrows indicate initial time for each cycle. b, Detail of current densities up to 24 h. c, Normalized data according to the total active metal content (Co, Ir or Ni/Fe), highlighting the superior activity of [Co-POM] per active site.

electrochemical data. There is a significant difference in the LSV data: the appearance of an additional precatalytic event in the Co_3O_4 electrodes (Supplementary Fig. 1), which is absent for the Co-POM catalysts.

Active surface area. To check if the different catalytic activity is only due to a different active surface area in the as-prepared materials, we carried out some additional characterization. First, we determined the BET surface area for all four catalysts (Supplementary Fig. 2). The results do not show significant differences, with very small BET areas for all materials, as expected, from 2 m^2 g^{-1} for IrO_2 and Cs[Co-POM], 11 m^2 g^{-1} for Ba[Co-POM] and 28 m^2 g^{-1} for Co_3O_4.

We also analysed the double-layer capacitance (C_{dl}) of the electrodes, which is expected to be linearly proportional to the effective active surface area (Supplementary Fig. 2). Although we cannot extract exact values due to the unknown behaviour of the catalyst and conducting support, we can easily estimate the relative surface areas for all electrodes. The results show how C_{dl} is two orders of magnitude higher for the Ba[Co-POM]/CP electrodes. This difference cannot be related to the BET surface area. These results indicate that the surface of the Ba[Co-POM] catalyst is intrinsically much more active towards water oxidation, which must be caused by the crystalline surface structure of this material and perhaps by the presence of the Ba^{2+} cations in close proximity.

Oxygen evolution and post-catalytic analysis. Oxygen evolution showed Faradaic production (>99%) for both Co-POM/CP electrodes, indicating a negligible contribution to the total measured currents from any other redox process (Supplementary Fig. 3). Oxygen evolution in the case of cobalt oxide is not Faradaic (~60–70%, Supplementary Fig. 4), providing additional evidence of a different electrochemical mechanism. Co_3O_4 is probably partially catalysing the oxidation of the CP component.

After 2 h electrolysis at j = 1 mA cm^{-2}, with an estimated turnover number (TON) of >10 (Supplementary section 'TON estimation'), we collected ex situ Raman and X-ray photoelectron spectroscopy (XPS) data (Supplementary Figs 5–7). These surface-sensitive characterization techniques are particularly useful for

detecting even traces of possible additional species generated in situ on a catalyst surface[43]. Comparative analyses do not show any significant differences between fresh and used materials, suggesting no change in the catalyst during oxygen production. The Raman spectra are undistinguishable. The XPS spectra are also identical at the W, P and Co edges. The O1s edge spectrum shows increased intensities for the higher energy peaks, which can be assigned to partial protonation of oxo sites. Thus, although we cannot rule out the possible participation of other species, the simplest explanation at present is that the [Co-POM] structure should be close to the true active species directly participating in the catalytic cycle. No additional contribution can be identified in the post-catalytic characterization. Infrared and X-ray powder diffraction data also support the bulk stability of the Co-POMs (Supplementary Figs 8 and 9). Furthermore, we found no leaching of the active species during working conditions, as confirmed by elemental analysis (ICP-OES) in H_2SO_4 (1 M) mother liquor after the corresponding 2 h electrolysis (Supplementary Table 1). Only low contents of counter-cations were detected for Cs[Co-POM], corresponding to a total loss of ~30% of the initial caesium and potassium content. We assigned this leaching to cation exchange by protons due to the highly acidic media, in good agreement with the XPS data. Barium leaching was not detected. We also carried out ICP-OES analysis of several fractions of the recovered catalyst (Supplementary Table 2). Although the carbon/binder content makes it difficult to obtain good-quality data, the results yielded consistent P/Co/W ratios for the used catalysts.

Long-term stability. The possibility to work at low overpotentials is essential for an energy-efficient power-to-fuels platform, because the extra potential needed to run the reaction represents a major energy loss. The excellent energy efficiency offered by our Ba[Co-POM] catalyst is also matched by good long-term catalytic stability. This was confirmed by chronoamperometric assays at $\eta = 250$ mV (Fig. 3a). For these experiments the electrodes were covered with a Nafion layer and with a frit to avoid fragmentation of the CP electrodes, which are mechanically unstable and tend to be expelled from the electrode pocket into the solution. The Ba[Co-POM]/CP electrodes showed a very high initial current density of >2 mA cm^{-2}. This current slowly decreases for the first hours to reach a stable current of ~0.36 mA cm^{-2} ($t = 4$ h), which is maintained for over 24 h without further significant changes (~0.35 mA cm^{-2} at $t = 24$ h), except those due to gas bubbles formation and diffusion. We assigned the initial decay to charge localization processes. We carried out an analogous experiment including periodic 20 min stops after each hour of electrolysis. In this case, the initial current density curve was identical in successive cycles (Fig. 3a and Supplementary Fig. 10). This result is not compatible with catalyst deactivation. The most plausible explanation is an increase in the resistance of the blend due to charge localization, what reduces the overall current density. At open-circuit potential, charges delocalize back to the initial state.

The stable current density values demonstrated for over one day by the Ba[Co-POM]/CP electrodes are unique among catalysts in the same conditions for the same catalyst weight (Fig. 3b). For the sake of comparison, we included IrO_2, Co_3O_4 and also two of the most efficient catalysts in alkaline and neutral conditions: $Ni_{0.9}Fe_{0.1}O_x$ (NiFe)[12] and CoP_i[21]. Obviously, none of these catalysts was optimized for our working conditions, but these experiments were worth conducting to further assess the distinct behaviour of the POMs. Only the CoP_i/CP initially showed a current density close to that of Ba[Co-POM]/CP (in the first hours), but continuous and irreversible deactivation brought its activity down to the level of the NiFe/CP. After 24 h, Ba[Co-POM]/CP promoted current densities three times higher than NiFe/CP and CoP_i/CP, four times higher than Co_3O_4/CP, and ten times higher than IrO_2/CP, even when containing a much lower total number of active sites, as discussed above. If we normalize the corresponding activity to the total metal content, the electrocatalytic activity of Ba[Co-POM]/CP is six times better than Cs[Co-POM]/CP and thirty times better than any other oxide (Fig. 3c), indicating a much faster turnover frequency per active site. In terms of oxygen evolution, Ba[Co-POM]/CP produces a total of 47 TON, clearly superior to the other catalysts: 8 (Cs[Co-POM]), 0.3 (CoP_i) or 0.1 (IrO_2).

At higher current densities (10 mA cm^{-2}), Ba[Co-POM]/CP still offers better performance (Supplementary Fig. 13), although the instability of the CP electrodes, as mentioned above, did not allow us to extend these studies for longer periods. Indeed, CP is suitable for fundamental studies, but it is not stable under OER conditions. Before the CP electrodes break down, after ~20 min, Ba[Co-POM]/CP is still competitive with IrO_2, suggesting the viability of this catalyst even at relatively high currents.

Conclusion

Oxygen evolution in strongly acidic conditions with earth-abundant catalysts is currently a major technological challenge. Our results show the excellent and unparalleled performance of Ba[Co-POM] for electrocatalytic water oxidation under these conditions. The significant influence of barium dications in the activity of the [Co-POM], when compared with the Cs^+ derivative, suggests that this strategy could also be useful in enhancing the performance of other water oxidation catalysts. POMs offer an intrinsic advantage in this regard, because their polyanionic nature makes it easy to selectively incorporate the desired ancillary counter-cations close to their active sites, without structurally or chemically affecting their appropriate environment.

We also need to highlight the non-innocent role of the CP component. Part of the better performance of the Co-POM/CP electrodes could arise from a better matching between the CP support and the Co-POM catalysts when compared with IrO_2. Indeed, an overall hydrophobic environment is known to enhance POM redox activity and stability[44,45]. According to our data, this also happens to be true for oxides, because the OER activity of the Co_3O_4/CP, CoP_i/CP and NiFe/CP electrodes is clearly superior to what has typically been reported for these oxides in acid. This suggests that the use of an insulating hydrocarbon binder and an appropriate conducting support could extend the use of classic metal oxides into acidic media OER catalysis. Such corrosion-protecting strategies have already been suggested by Schaak and co-authors[25]. Therefore, tuning the hydrophobic/hydrophilic character of composite electrodes may open fascinating opportunities for low-cost acid water electrolysis.

Methods

Synthesis. Materials and detailed methods are further described in the Supplementary Information. $Na_8K_8[Co_9(H_2O)_6(OH)_3(HPO_4)_2(PW_9O_{34})_3]\cdot xH_2O$ (1) was obtained following a method described in the literature[46]. $Cs_{15}K[Co_9(H_2O)_6(OH)_3(HPO_4)_2(PW_9O_{34})_3]\cdot 28H_2O$ (Cs[Co-POM]) and $Ba_8[Co_9(H_2O)_6(OH)_3(HPO_4)_2(PW_9O_{34})_3]\cdot 55H_2O$ (Ba[Co-POM]) were prepared by metathesis with an excess of CsCl or $BaCl_2$. The presence of the $[Co_9(H_2O)_6(OH)_3(HPO_4)_2(PW_9O_{34})_3]^{16-}$ anion in Cs[Co-POM] and Ba[Co-POM] was confirmed by its signature infrared spectra (Supplementary Fig. 8). In POM chemistry, the infrared bands represent a reliable fingerprint for the molecular structure. Cation content was estimated by ICP-OES and energy-dispersive X-ray spectroscopy (EDX). Water content was determined by thermogravimetric analysis (TGA) (Supplementary Figs 11 and 12). Cs[Co-POM].$28H_2O$ $M_w = 10{,}107.15$. Elemental analyses, Calc.: Cs, 19.73; K, 0.40; Co, 5.25; P, 1.53; W, 49,11. Exp.: Cs, 19.51; K, 0.52; Co, 5.40; P, 1.39; W, 49.30. Ba[Co-POM].$55H_2O$ $M_w = 9659.40$. Elemental analyses, Calc.: Ba, 11.37; K, 0.00; Co, 5.49; P, 1.60; W, 51.39. Exp.: Ba, 11.51; K, <0.1; Co, 5.35; P, 1.58; W, 51.06.

Electrochemistry. Electrochemical experiments were performed with a Biologic SP-150 potentiostat. Ohmic drop was compensated using the positive feedback compensation implemented in the instrument. All experiments were performed with a three-electrode configuration using H_2SO_4 (1 M) as electrolyte solution, employing a platinum mesh counter electrode, a Ag/AgCl (KCl 3.5 M) reference electrode and a CP working electrode (surface area = 0.07 cm^2). The CP mixtures

were prepared in a mortar by mixing amorphous CP and the desired material in the corresponding ratio by weight. This modified CP mixture was used to fill the CP electrode. Bulk water electrolysis and LSV were performed with an ALS RRDE-3A set-up, using a CP rotating disk electrode (surface area = 0.07 cm^2) at 1,600 and 500 r.p.m., respectively. All LSV experiments were carried out with a 1 mV s^{-1} scan rate. Steady-state current data for Tafel analyses were obtained after the needed waiting time for stabilization of the current at each overpotential (at least 10 min) in an H-cell. For long-term electrolysis (over 1 h) the CP pocket was covered with a Nafion ink (4 μl at 5%) and with a glass frit (P0, 1 mm thick) on top to avoid mechanical losses of the CP into the solution.

Oxygen evolution was detected with an Ocean Optics NeoFOX oxygen sensing system equipped with a FOXY probe. The FOXY probe was calibrated with a two point calibration, fixing 0% O_2 under N_2 flow and 20.9% O_2 in air. The experiments were carried out in an H-cell, with the anode and cathode compartments separated by a porous frit. The FOXY probe was inserted into the gas space of the anodic compartment ($V_{GAS\ SPACE} \approx 4.9$ ml). The solution was completely deaerated by purging with N_2 before starting the experiment, for at least 1 h. N_2 flow was removed and a base line of 10 min was recorded before starting the chronoamperometry. The mols of O_2 generated during the electrochemical experiment were calculated with the following equation, considering ideal gas behaviour:

$$n_{O_2} = \frac{\%O_2 \cdot P_{TOTAL} \cdot V_{GAS\ SPACE}}{100 \times R \times T}$$

where $\%O_2$ is given by the FOXY probe, P_{TOTAL} is 1 atm, $V_{GAS\ SPACE}$ (litres) is measured for each experiment, R is 0.082 (atm l/K mol) and T is 298 K. The faradaic oxygen production curve was calculated taking into account the charge data from the chronoamperometry experiment as described in the following equation:

$$n_{O_2} = \frac{Q}{n_e \cdot F}$$

where Q (C) is the charge passed through the system, $n_e = 4$ is the number of electrons needed to generate one molecule of O_2, and F is the Faraday constant (96,485 C mol^{-1}).

pH was measured for each experiment using an 877 Titrino Plus pH-probe (Metrohm), calibrated weekly. The pH value was used to calculate the thermodynamic water oxidation potential ($E^0_{H_2O/O_2}$) using the Nerst equation:

$$E^0_{H_2O/O_2} = 1.229 - 0.059\ pH(V)\ vs\ NHE\ at\ 25\ °C$$

The overpotential η was calculated by subtracting the thermodynamic water oxidation potential to the applied potential E_{app}:

$$\eta = E_{app} - E^0_{H_2O/O_2}$$

All potentials were converted to the NHE reference scale using $E_{NHE} = E_{Ag/AgCl} + 0.205$ (V). All current densities were calculated based on the geometrical surface area of the electrodes. Onset potentials in Table 1 were estimated from the intersection point between the tangent lines of the Faradaic (above j = 0.2 mA cm^{-2}) and non-Faradaic (below η = −0.1 V) currents (Supplementary Fig. 1)

Recovery of the catalysts. After electrochemical experiments, the POM/CP blend (40 mg) was suspended in acetone (30 ml) and sonicated for 5 min. The supernatant liquid (containing carbon black and the organic oil binder) was decanted, retaining the POM catalyst in the beaker. This procedure was repeated 10 times to obtain a clean catalyst sample. The supernatant fraction was also collected for additional analysis (Supplementary Table 2).

Data availability. Additional methods and materials characterization are available in the Supplementary Information. Supplementary figures include electrochemical (Supplementary Figs 1, 2, 10 and 13), oxygen evolution (Supplementary Figs 3 and 4), Raman spectroscopy (Supplementary Fig. 5), XPS (Supplementary Figs 6 and 7), infrared spectroscopy (Supplementary Fig. 8), powder X-ray diffraction (Supplementary Figs 9 and 10) and thermogravimetry (Supplementary Figs 11 and 12) data. Supplementary tables include elemental analyses (Supplementary Tables 1 and 2) and TON estimations (Supplementary Tables 3 and 4).

References

1. McKone, J. R., Lewis, N. S. & Gray, H. B. Will solar-driven water-splitting devices see the light of day? Chem. Mater. 26, 407–414 (2014).
2. Ursua, A., Gandia, L. M. & Sanchis, P. Hydrogen production from water electrolysis: current status and future trends. Proc. IEEE 100, 410–426 (2012).
3. Staszak-Jirkovsky, J. et al. Design of active and stable Co-Mo-Sx chalcogels as pH-universal catalysts for the hydrogen evolution reaction. Nat. Mater. 15, 197–203 (2016).
4. Andreiadis, E. S. et al. Molecular engineering of a cobalt based electrocatalytic nanomaterial for H_2 evolution under fully aqueous conditions. Nat. Chem. 5, 48–53 (2013).
5. Hinnemnann, B. et al. Biomimetic hydrogen evolution: MoS_2 nanoparticles as catalysts for hydrogen evolution. J. Am. Chem. Soc. 127, 5308–5309 (2005).
6. McCrory, C. C. L. et al. Benchmarking hydrogen evolving reaction and oxygen evolving reaction electrocatalysts for solar water splitting devices. J. Am. Chem. Soc. 137, 4347–4357 (2015).
7. Harriman, A., Pickering, I. J., Thomas, J. M. & Christensen, P. A. Metal-oxides as heterogeneous catalysts for oxygen evolution under photochemical conditions. J. Chem. Soc. Faraday Trans. 84, 2795–2806 (1988).
8. Sardar, K. et al. Water-splitting electrocatalysis in acid conditions using ruthenate-iridate pyrochlores. Angew. Chem. Int. Ed. 53, 10960–10964 (2014).
9. Harriman, A. Prospects for conversion of solar energy into chemical fuels: the concept of a solar fuels industry. Phil. Trans. R. Soc. A 371, 20110415 (2013).
10. Yu, E. H., Wang, X., Krewer, U., Li, L. & Scott, K. Direct oxidation alkaline fuel cells: from materials to systems. Energy Environ. Sci. 5, 5668–5680 (2012).
11. Corrigan, D. A. The catalysis of the oxygen evolution reaction by iron impurities in thin film nickel oxide electrodes. J. Electrochem. Soc. 134, 377–384 (1987).
12. Trotochaud, L., Ranney, J. K., Williams, K. N. & Boettcher, S. W. Solution-cast metal oxide thin film electrocatalysts for oxygen evolution. J. Am. Chem. Soc. 134, 17253–17261 (2012).
13. Smith, R. D. L. et al. Photochemical route for accessing amorphous metal oxide materials for water oxidation catalysis. Science 340, 60–63 (2013).
14. Gerken, J. B., Shaner, S. E., Massé, R. C., Porubsky, N. J. & Stahl, S. S. A survey of diverse earth abundant oxygen evolution electrocatalysts showing enhanced activity from Ni–Fe oxides containing a third metal. Energy Environ. Sci. 7, 2376–2382 (2014).
15. Galan-Mascaros, J. R. Water oxidation at electrodes modified with earth-abundant transition-metal catalysts. ChemElectroChem 2, 37–50 (2015).
16. Suntivich, J., May, J., Gasteiger, H. A., Goodenough, J. B. & Shao-Horn, Y. A perovskite oxide optimized for oxygen evolution catalysis from molecular orbital principles. Science 334, 1383–1385 (2011).
17. Zhang, B. et al. Homogeneously dispersed multimetal oxygen-evolving catalysts. Science 352, 333–337 (2016).
18. McCrory, C. C. L., Jung, S., Peters, J. C. & Jaramillo, T. F. Benchmarking heterogeneous electrocatalysts for the oxygen evolution reaction. J. Am. Chem. Soc. 135, 16977–16987 (2013).
19. Gorlin, M. et al. Tracking catalyst redox states and reaction dynamics in Ni–Fe oxyhydroxide oxygen evolution reaction electrocatalysts: the role of catalyst support and electrolyte pH. J. Am. Chem. Soc. 139, 2070–2082 (2017).
20. Gerken, J. B. et al. Electrochemical water oxidation with cobalt-based electrocatalysts from pH 0–14: the thermodynamic basis for catalyst structure, stability, and activity. J. Am. Chem. Soc. 133, 14431–14442 (2011).
21. Kanan, M. W. & Nocera, D. G. In situ formation of an oxygen-evolving catalyst in neutral water containing phosphate and Co^{2+}. Science 321, 1072–1075 (2008).
22. Surendranath, Y., Lutterman, D. A., Liu, Y. & Nocera, D. G. Nucleation, growth, and repair of a cobalt-based oxygen evolving catalyst. J. Am. Chem. Soc. 134, 6326–6336 (2012).
23. Huynh, M., Bediako, D. K. & Nocera, D. G. A functionally stable manganese oxide oxygen evolution catalyst in acid. J. Am. Chem. Soc. 136, 6002–6010 (2014).
24. Frydendal, R., Paoli, E. A., Chorkendorff, I., Rossmeisl, J. & Stephens, I. E. L. Toward an active and stable catalyst for oxygen evolution in acidic media: Ti-stabilized MnO_2. Adv. Energy Mater. 5, 1500991 (2015).
25. Mondschein, J. S. et al. Crystalline cobalt oxide films for sustained electrocatalytic oxygen evolution under strong acidic conditions. Chem. Mater. 29, 950–957 (2017).
26. Bloor, L. G., Molina, P. I., Symes, M. D. & Cronin, L. Low pH electrolytic water splitting using earth-abundant metastable catalysts that self-assemble in situ. J. Am. Chem. Soc. 136, 3304–3311 (2014).
27. Yin, Q. et al. A fast soluble carbon-free molecular water oxidation catalyst based on abundant metals. Science 328, 342–345 (2010).
28. Lv, H. J. et al. An exceptionally fast homogeneous carbon-free cobalt-based water oxidation catalyst. J. Am. Chem. Soc. 136, 9268–9271 (2014).
29. Lv, H. J. et al. Polyoxometalate water oxidation catalysts and the production of green fuel. Chem. Soc. Rev. 41, 7572–7589 (2012).
30. Goberna-Ferron, S., Vigara, L., Soriano-Lopez, J. & Galan-Mascaros, J. R. Identification of a nonanuclear $\{Co^{II}_9\}$ polyoxometalate cluster as a homogeneous catalysts for water oxidation. Inorg. Chem. 51, 11707–11715 (2012).
31. Stracke, J. J. & Finke, R. C. Electrocatalytic water oxidation beginning with the cobalt polyoxometalate $[Co_4(H_2O)_2(PW_9O_{34})_2]^{10-}$: identification of heterogeneous CoO_x as the dominant catalyst. J. Am. Chem. Soc. 133, 14872–14875 (2011).

32. Natali, M. et al. Is $[Co_4(H_2O)_2([\alpha]\text{-}PW_9O_{34})_2]^{10-}$ a genuine molecular catalyst in photochemical water oxidation? Answers from time-resolved hole scavenging experiments. Chem. Commun. 48, 8808–8810 (2012).
33. Stracke, J. J. & Finke, R. C. Water oxidation catalysis beginning with 2.5 μM $[Co_4(H_2O)_2(PW_9O_{34})_2]^{10-}$: investigation of the true electrochemically driven catalyst at ≥600 mV overpotential at a glassy carbon electrode. ACS Catal. 3, 1209–1219 (2013).
34. Vickers, J. W. et al. Differentiating homogeneous and heterogeneous water oxidation catalysis: confirmation that $[Co_4(H_2O)_2(\alpha\text{-}PW_9O_{34})_2]^{10-}$ is a molecular water oxidation catalyst. J. Am. Chem. Soc. 135, 14110–14118 (2013).
35. Stracke, J. J. & Finke, R. C. Water oxidation catalysis beginning with $Co_4(H_2O)_2(PW_9O_{34})_2{}^{10-}$ when driven by the chemical oxidant ruthenium(III) tris(2,2′-bipyridine): stoichiometry, kinetic, and mechanistic studies en route to identifying the true catalyst. ACS Catal. 4, 79–89 (2014).
36. Natali, M. et al. Photo-assisted water oxidation by high-nuclearity cobalt-oxo cores: tracing the catalyst fate during oxygen evolution turnover. Green Chem. 19, 2416–2426 (2017).
37. Goberna-Ferrón, S., Soriano-López, J., Galán-Mascarós, J. R. & Nyman, M. Solution speciation and stability of cobalt-polyoxometalate water oxidation catalysts by X-ray scattering. Eur. J. Inorg. Chem. 2015, 2833–2840 (2015).
38. Soriano-López, J. et al. Cobalt polyoxometalates as heterogeneous water oxidation catalysts. Inorg. Chem. 52, 4753–4755 (2013).
39. Huynh, M., Shi, C., Billinge, S. J. L. & Nocera, D. G. Nature of activated manganese oxide for oxygen evolution. J. Am. Chem. Soc. 137, 14887–14904 (2015).
40. Kushner-Lenhoff, M. N., Blakemore, J. D., Schley, N. D., Crabtree, R. H. & Brudvig, G. W. Effects of aqueous buffers on electrocatalytic water oxidation with an iridium oxide material electrodeposited in thin layers from an organometallic precursor. Dalton Trans. 42, 3617–3622 (2013).
41. Ouattara, L., Fierro, S., Frey, O., Koudelka, M. & Comninellis, C. Electrochemical comparison of IrO_2 prepared by anodic oxidation of pure iridium and IrO_2 prepared by thermal decomposition of H_2IrCl_6 precursor solution. J. Appl. Electrochem. 39, 1361–1367 (2009).
42. Seitz, L. C. et al. A highly active and stable $IrO_x/SrIrO_3$ catalyst for the oxygen evolution reaction. Science 353, 1011–1014 (2016).
43. Ahn, H. S. & Tilley, T. D. Electrocatalytic water oxidation at neutral pH by a nanostructured $Co(PO_3)_2$ anode. Adv. Funct. Mater. 23, 227–233 (2013).
44. Carraro, M., Sandei, L., Sartorel, A., Scorrano, G. & Bonchio, M. Hybrid polyoxotungstates as second-generation POM-based catalysts for microwave-assisted H_2O_2 activation. Org. Lett. 8, 3671–3674 (2006).
45. Berardi, S. et al. Polyoxometalate-based N-heterocyclic carbene (NHC) complexes for palladium-mediated C–C coupling and chloroaryl dehalogenation catalysis. Chem. Eur. J. 16, 10662–10666 (2010).
46. Galan-Mascaros, J. R., Gomez-Garcia, C. J., Borras, J. J. & Coronado, E. High nuclearity magnetic clusters: magnetic properties of a nine cobalt cluster encapsulated in a polyoxometalate $[Co_9(OH_2)_3(HO)_3(HPO_4)_2(PW_9O_{34})_3]^{16-}$. Adv. Mater. 6, 221–223 (1994).

Acknowledgements

This work was supported by the European Union (project ERC StG, grant CHEMCOMP, no. 279313), the Spanish Ministerio de Economía y Competitividad (MINECO; through projects CTQ2015-71287-R, CTQ2014-52774-P and the Severo Ochoa Excellence Accreditation 2014-2018 SEV-2013-0319), the Generalitat de Catalunya (2014-SGR-797 and 2014SGR-199) and the CERCA Programme/Generalitat de Catalunya.
J.M.P. acknowledges the ICREA Foundation for an ICREA Academia award.
M.B.A. acknowledges the Generalitat Catalana (AGAUR) for a predoctoral fellowship.
The authors also thank Á. Reyes-Carmona for discussions.

Author contributions

J.R.G.-M. proposed the concept. J.R.G.-M., M.B.-A. and J.S.-L. designed the experiments. M.B.-A. and J.S.-L. performed the experiments. All authors participated in data analysis and co-wrote the manuscript.

Additional information

Supplementary information is available in the online version of the paper. Reprints and permissions information is available online at www.nature.com/reprints. Publisher's note: Springer Nature remains neutral with regard to jurisdictional claims in published maps and institutional affiliations. Correspondence and requests for materials should be addressed to J.R.G.-M.

Competing financial interests

The authors declare no competing financial interests.